

Ab initio molecular dynamics of paramagnetic uranium mononitride (UN) using disordered local moments

Mohamed AbdulHameed^a, Benjamin Beeler^{a,b,*}

^a*Department of Nuclear Engineering, North Carolina State University, Raleigh, NC 27695*

^b*Idaho National Laboratory, Idaho Falls, ID 83415*

Abstract

This work presents an investigation of the thermophysical properties of paramagnetic uranium mononitride (UN) using *ab initio* molecular dynamics (AIMD) simulations combined with the disordered local moment (DLM) approach. This methodology accurately captures the high-temperature paramagnetic state of UN, addressing the limitations of standard density functional theory (DFT) models. The AIMD+DLM model consistently predicts a cubic crystal structure for UN across all considered temperatures, aligning with experimental observations of its paramagnetic phase. Key thermophysical properties, including the lattice parameter and specific heat capacity, are computed and compared to experimental data. The calculated lattice parameter is somewhat underestimated relative to the empirical correlation, consistent with prior studies modeling UN as a ferromagnetic (FM) or anti-ferromagnetic (AFM) material. The specific heat capacity exhibits overestimation at low temperatures (300–500 K) and slight underestimation at higher temperatures, while closely following the experimental trend. These results highlight the accuracy and utility of the AIMD+DLM framework in modeling paramagnetic materials, which can offer insights into the influence of the magnetic state on the behavior of nuclear fuels at high temperatures.

Keywords: uranium nitride, ab initio molecular dynamics, disordered local moments, paramagnetic state, thermophysical properties

¹ 1. Introduction

² Uranium mononitride (UN) is recognized as a promising advanced nuclear fuel, offering
³ several advantages including high fissile density, excellent thermal conductivity, compatibility
⁴ with various cladding materials, and potential for extended fuel cycles [1, 2]. Despite
⁵ these benefits, certain properties of UN remain unexplored, particularly the influence of its
⁶ magnetic state on various material characteristics. This is due to the challenges associated
⁷ with accurately simulating its magnetic states using density functional theory (DFT).

⁸ Below a Néel temperature, T_N , of about 53 K, UN has an antiferromagnetic (AFM) state
⁹ of type I with the spins of U atoms aligned along the [001] direction [3]. The expected
¹⁰ tetragonal distortion in this type of magnetic order is minimal for UN ($|c/a - 1| = 6.5 \times 10^{-4}$

*Corresponding author

Email address: bwbeeler@ncsu.edu (Benjamin Beeler)

11 at 4.2 K [4]) and it is even debated whether a tetragonal distortion exists or not [4]. Above
12 T_N , UN transitions to a paramagnetic material and assumes a fully cubic NaCl-type crystal
13 structure.

14 Paramagnetism is a finite-temperature phenomenon arising from thermal and quantum
15 fluctuations, characterized by random, non-collinear local magnetic moments that persist
16 above the magnetic transition temperature. In this state, these moments fluctuate both in
17 time and space due to temperature-driven spin excitations, resulting in zero time-averaged
18 net magnetization in the absence of an external magnetic field [5]. The time scale of these
19 fluctuations, known as the spin decoherence time, is on the order of 10 fs [6], representing the
20 temporal resolution required to correctly simulate spin dynamics in paramagnetic materials.
21 Compared to ordered magnetic states, where excitations tied to spin-wave frequencies occur
22 on a scale of ~ 100 fs [5], the magnetic degrees of freedom in paramagnetic materials are
23 significantly faster. While the paramagnetic state is ergodic over long timescales, it exhibits
24 transient correlations and non-uniform sampling of the phase space over shorter timescales
25 [7, 5]. This can be appropriately termed quasi-ergodic or slowly ergodic behavior.

26 First-principles methods face significant challenges in accurately describing paramag-
27 netism due to both fundamental and practical limitations. Fundamentally, these meth-
28 ods rely on adiabatic decoupling of magnetic and vibrational degrees of freedom [5] and
29 approximations like the local spin density approximation (LSDA), which can only model
30 ground-state properties and static spin configurations [8]. Consequently, they fail to capture
31 dynamic spin fluctuations and strong electron correlations typical of paramagnetic materials
32 [9]. While advanced approaches like DFT+ U and the dynamical mean field theory (DMFT)
33 improve correlation modeling, DFT+ U cannot represent the paramagnetic state [10, 11], and
34 DMFT struggles with short-range order near the magnetic transition [5]. Combined meth-
35 ods such as DFT+DMFT offer more accurate descriptions but are computationally intensive
36 [9, 6].

37 Practically, simulating the high-temperature paramagnetic state with standard *ab initio*
38 molecular dynamics (AIMD) is challenging due to mismatched timescales between atomic
39 and spin dynamics. AIMD typically requires simulation times of 3–5 ps with a time step of
40 1 fs, while the spin decoherence time is ~ 10 fs [6, 5]. As a result, spin configurations evolve
41 more slowly than atomic configurations on short timescales but can change significantly over
42 the duration of an MD simulation. This discrepancy makes it difficult to separate magnetic
43 and vibrational degrees of freedom, leading to the breakdown of adiabatic decoupling.

44 The disordered local moment (DLM) approach combined with AIMD effectively mod-
45 els magnetic fluctuations and the quasi-static behavior of the paramagnetic state [5]. This
46 AIMD+DLM framework has been used to study the influence of the paramagnetic state
47 on properties of materials with known strong coupling between magnetic and lattice de-
48 grees of freedom. Steneteg *et al.* [6] introduced this method to calculate the equation of
49 state and bulk modulus of CrN, demonstrating no collapse of the bulk modulus across the
50 antiferromagnetic-to-paramagnetic transition. Mozafari *et al.* [12] extended this framework
51 to compute the temperature-dependent elastic constants of CrN. Alling *et al.* [13] utilized
52 AIMD+DLM to study the impact of lattice vibrations on magnetic and electronic properties
53 of paramagnetic iron.

54 Standard 0 K DFT studies of UN using generalized gradient approximation (GGA)
55 exchange-correlation functionals have found that the ferromagnetic (FM) order is lower in

56 energy than AFM UN [14] in contradiction to experimental observations. In these calcu-
57 lations, FM UN is fully cubic, and AFM UN is characterized by a tetragonal distortion. When
58 an effective Hubbard $U = 1.9$ eV is used along with the GGA functionals, AFM UN becomes
59 more energetically favorable than FM UN, and AFM UN is characterized by an orthorhom-
60 bic distortion [15]. Furthermore, Kocevski *et al.* [14] have shown that when AFM UN is
61 modeled using DFT+ U , it exhibits imaginary phonon frequencies, indicating a dynamically
62 unstable crystal structure.

63 This work presents the first application of the AIMD+DLM framework to simulate the
64 paramagnetic state of UN. By treating UN as a paramagnetic material, we calculate several
65 thermophysical properties and compare them with available experimental data. To the best
66 of our knowledge, only one AIMD study on UN has been reported in the literature. In that
67 study, Kocevski *et al.* [16] employed FM and AFM models to investigate the thermophysical
68 and elastic properties of UN. However, these models do not accurately represent the high-
69 temperature paramagnetic state of UN, highlighting the significance of our study.

70 2. Computational details

71 AIMD simulations in this study were performed using the Vienna *ab initio* Simulation
72 Package (VASP) [17, 18, 19], employing the Perdew-Burke-Ernzerhof (PBE) generalized
73 gradient approximation (GGA) for the exchange-correlation functional [20]. Projector-
74 augmented wave (PAW) pseudopotentials were used for uranium and nitrogen. The valence
75 electron configuration of uranium is $6s^2 6p^6 6d^2 5f^2 7s^2$ (14 electrons), while that of nitro-
76 gen is $2s^2 2p^3$ (5 electrons). To treat partial electronic occupancies, the first-order smearing
77 method of Methfessel and Paxton [21] was employed with a smearing width of 0.1 eV.

78 The UN system is modeled using $3 \times 3 \times 3$ supercells containing 216 atoms. A plane-
79 wave cutoff energy of 520 eV is used, and the energy convergence criterion for electronic
80 optimization is set to 10^{-3} eV. Brillouin-zone integrations are performed at the Γ point. The
81 initial structure was constructed with an AFM configuration, but the system transitioned to
82 an FM state almost instantaneously upon relaxation. Simulation of a smaller $2 \times 2 \times 2$ AFM
83 UN supercell showed that the AFM state was stable for 1 ps at 300 K. However, for the larger
84 $3 \times 3 \times 3$ supercell, the AFM state could not be sustained at any temperature. It should be
85 noted that this is in contradiction to the findings of Kocevski [16]. The $3 \times 3 \times 3$ supercells
86 in this work are equilibrated in the *NPT* ensemble at zero pressure and temperatures of
87 300, 500, 1000, 1500, and 2000 K over a period of 1 ps using standard spin-polarized AIMD
88 simulations, in which UN is in the FM state. Subsequently, the disordered local moment
89 (DLM) model is applied.

90 In the DLM model, it is assumed that the magnetic moments undergo random reori-
91 entation over a characteristic spin-flip time, $t_{SF} = 5$ fs. The spin-flip time is recommended to
92 be much shorter than the spin decoherence time because a slow spin-dynamics model would
93 lead to large spin-lattice correlations if the nuclei were allowed to relax in response to the
94 static local magnetic moment distribution [6]. The simulation is initialized by assigning ran-
95 domly oriented collinear local magnetic moments to U atoms, under the constraint that the
96 net magnetic moment of the supercell is zero. Collinear spin-polarized AIMD simulations
97 are then performed for t_{SF}/t_{MD} time steps, where $t_{MD} = 1$ fs is the length of a single AIMD
98 time step. After each spin-flip interval, the collinear spins are reassigned randomly while the

99 lattice positions and velocities remain unchanged, and the process is repeated iteratively.
 100 During each spin-flip interval, the magnitudes of the local magnetic moments are allowed to
 101 evolve self-consistently. The goal is to achieve a magnetic state that exhibits no order on
 102 either the supercell length scale or the simulation time scale. Note that the DLM approach
 103 alone gives a state of temporarily broken ergodicity, where the system is stuck for a time
 104 equal to t_{SF} in a single point in the phase space [7, 5]. However, the occasional spin flips
 105 motivated by the self-consistent solution make the system achieve the desired quasi-ergodic
 106 behavior of the paramagnetic state. Non-collinear magnetic moments as well as spin-orbit
 107 coupling are not treated in this work. The DLM iterations are continued for 3 ps, which
 108 corresponds to 600 spin flips. In total, the 1-ps FM run and the 3-ps DLM run give a total
 109 simulation time of 4 ps. A Bash/Python script that implements the DLM method using
 110 VASP can be found in the Supplementary Information.

111 To demonstrate the accuracy of the AIMD+DLM model of UN, its lattice constant and
 112 specific heat capacity are calculated and compared to available experimental data. The
 113 lattice constant is calculated by averaging the supercell dimensions along the x -, y - and
 114 z directions over the whole simulation time. UN behaves as a metallic solid [22], and its
 115 specific heat capacity is a sum of lattice and electronic specific heats: $C_P = C_{\text{lat}} + C_{\text{elec}}$. The
 116 total energies of supercells are averaged over the last 2.5 ps for all temperatures. Then, the
 117 averaged values are fitted to a third-degree polynomial of the form:

$$E = a + bT + cT^2 + dT^3. \quad (1)$$

118 The lattice specific heat capacity can then be calculated as:

$$C_{\text{lat}} = \frac{1}{n} \frac{dE}{dT} = \frac{1}{n} (b + 2cT + 3dT^2), \quad (2)$$

119 where n is the number of moles. This method was employed due to the limited number of
 120 temperature points, which prohibits the use of a finite difference approach. The electronic
 121 specific heat is estimated from [23]:

$$C_{\text{elec}} = \gamma T, \quad (3)$$

122 where γ is the electronic specific heat coefficient ($\text{J/mol}\cdot\text{K}^2$), whose value is $\gamma = 3.7 \text{ mJ/mol}\cdot$
 123 K^2 [4, 24].

124 3. Results

125 The total system potential energy of UN as a function of time at 300 and 2000 K are
 126 shown in Fig. 1. In Fig. 1a, it can be seen that for low temperatures, the potential energy of
 127 the FM state (the first 1 ps in the figure) is lower than that of the DLM state (the last 3 ps
 128 in the figure). With increasing temperature, e.g., Fig. 1b, the potential energies of the two
 129 states become comparable. Despite the large thermal fluctuations in the potential energy
 130 at 2000 K, its running average is seen to be well-converged during the last 1.5 ps of the
 131 simulation time.

132 Figure 2 shows the system-wide magnetic moment and the magnetic moment of an arbit-
 133 rarily chosen U atom in the supercell as a function of time. In Fig. 2a, it can be seen that
 134 the average magnetic moment per U atom at 500 K is practically conserved and fluctuates

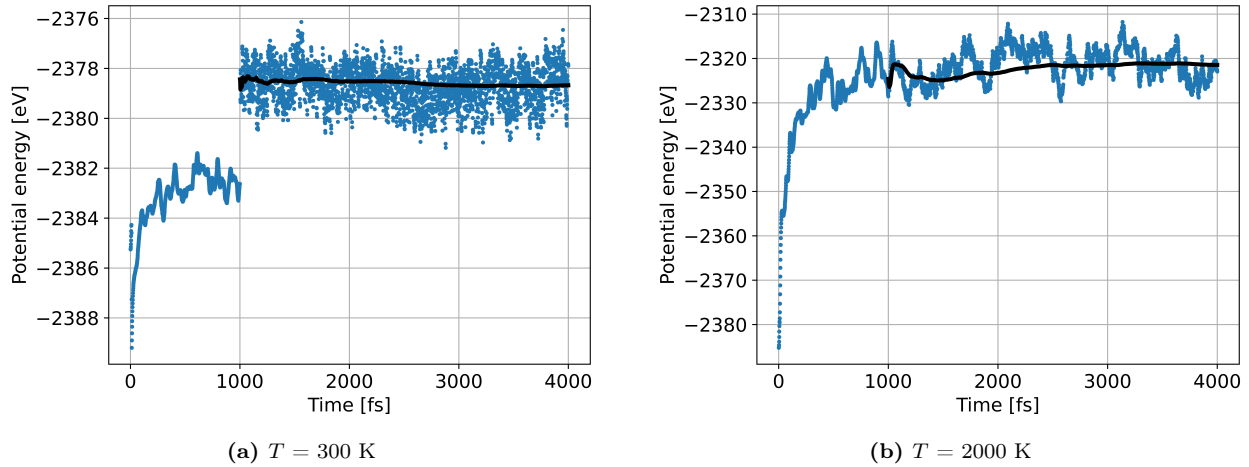


Figure 1: (Color online) Potential energy of the supercell at (a) 300 K and (b) 2000 K. Black thick lines correspond to running averages.

about zero during the whole time of the DLM run, where the fluctuations are bound between $\pm 0.25 \mu_B$. The magnetic moment of an arbitrarily chosen U atom at 1000 K is shown in Fig. 2b. It fluctuates about a running average of zero where the fluctuations are mostly between $\pm 1.25 \mu_B$, which coincides with the per-U magnetic moment of FM UN at 0 K [14], but is larger than $\mu = 0.75 \mu_B$ —the experimental per-U magnetic moment of AFM UN below T_N [3]. Similar trends have been observed at all considered temperatures. Thus, a consistent qualitative description of the magnetically disordered paramagnetic state of UN is obtained.

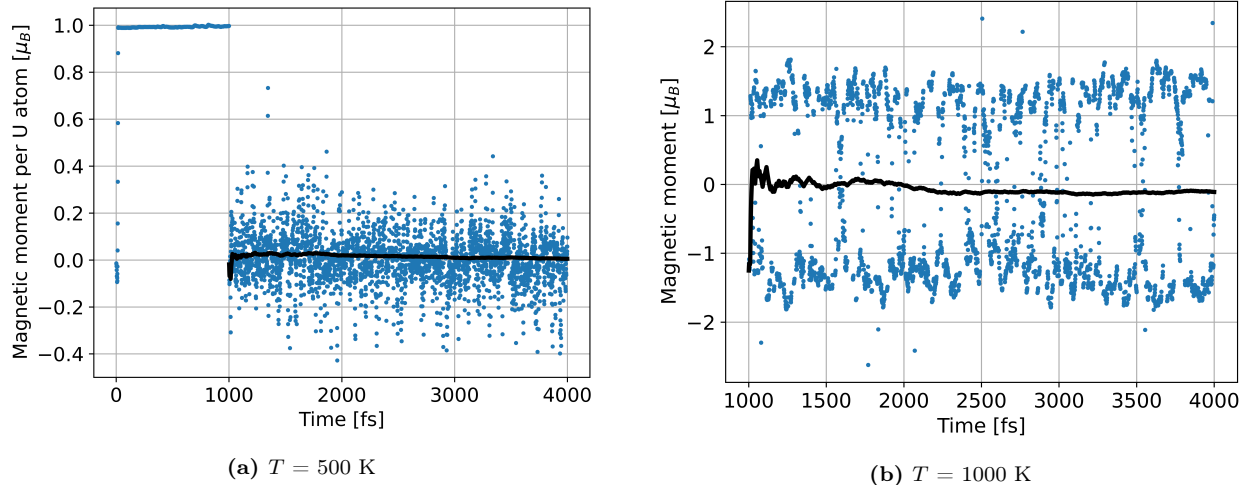


Figure 2: (Color online) **(a)** Magnetic moment per U atom at 500 K averaged over the supercell. **(b)** Magnetic moment of an arbitrarily chosen U atom at 1000 K for only the DLM part of the simulation. Black thick lines correspond to running averages.

To converge to the magnetic ground state, the VASP documentation recommends setting the initial magnetic moments slightly larger than the expected values. In our calculations, we set the initial magnetic moments per U atom to $\pm 5 \mu_B$. To determine if initial magnetic

moments affect magnetic moment oscillations, we performed AIMD+DLM calculations at 300 K for 0.5 ps following a 1-ps FM equilibration. Initial magnetic moments per U atom were set to $\pm 1 \mu_B$ instead of $\pm 5 \mu_B$. The per-atom magnetic moments fluctuated between $\pm 1.25 \mu_B$, indicating that the prescribed magnitude of the magnetic moments does not influence the magnitude of the observed fluctuations.

The lattice parameter and structure angles are shown in Fig. 3 as a function of time at 300 and 1500 K. The running averages of the UN unit cell's lengths and angles nearly coincide at lower temperatures as is obvious in Figs. 3a and 3b, respectively. As expected, deviations from the purely cubic structure increase with increasing temperature due to thermal fluctuations, but the deviations are relatively small and converge to the purely cubic case when the DLM run is well-converged, as can be seen in Figs. 3c and 3d for $T = 1500$ K. Thus, it can be concluded that the DLM model of paramagnetic UN predicts it to be purely cubic at all temperatures, in agreement with experimental observations. The reason why the DLM gives a cubic structure and not the tetragonal/orthorhombic distortion expected from a static AFM order [25] can be explained as follows: the spin-flip time interval, $t_{SF} = 5$ fs, is so short that the nuclei do not have sufficient time to adjust their positions for the current distribution of magnetic moments and move toward the positions that would give a tetragonal/orthorhombic distortion [6].

The lattice parameter of UN obtained from AIMD simulations is presented in Fig. 4a. The calculated lattice parameter is somewhat underestimated compared to the empirical correlation reported by Hayes *et al.* [26], and is very close to that calculated by Kocevski *et al.* [16] for AFM UN using AIMD. The standard deviation of the lattice parameter exhibits a systematic increase with temperature, attributed to enhanced thermal fluctuations. The temperature dependence of the lattice parameter has been fitted to the following polynomial expression:

$$a(T) = 4.862 + 1.593 \times 10^{-5}T + 8.719 \times 10^{-9}T^2, \quad (4)$$

with a coefficient of determination, $R^2 = 99.6\%$.

The calculated specific heat capacity, C_P , of UN is presented in Fig. 4b, alongside a comparison with the empirical correlation provided by Hayes *et al.* [27] and the AIMD data calculated by Kocevski *et al.* [16] for AFM UN. In the 300–500 K temperature range, C_P is overestimated compared to experimental data and Kocevski's calculation. The reason for this overestimation is the lack of an energy data point at $T < 300$ K, which is needed to obtain a more accurate energy derivative at 300 K. At higher temperatures, $T > 500$ K, while C_P is slightly underestimated, it closely follows the same trend as the empirical correlation. This is not the case for Kocevski's calculation which follows a linear increase that would underestimate C_P if extrapolated to higher T .

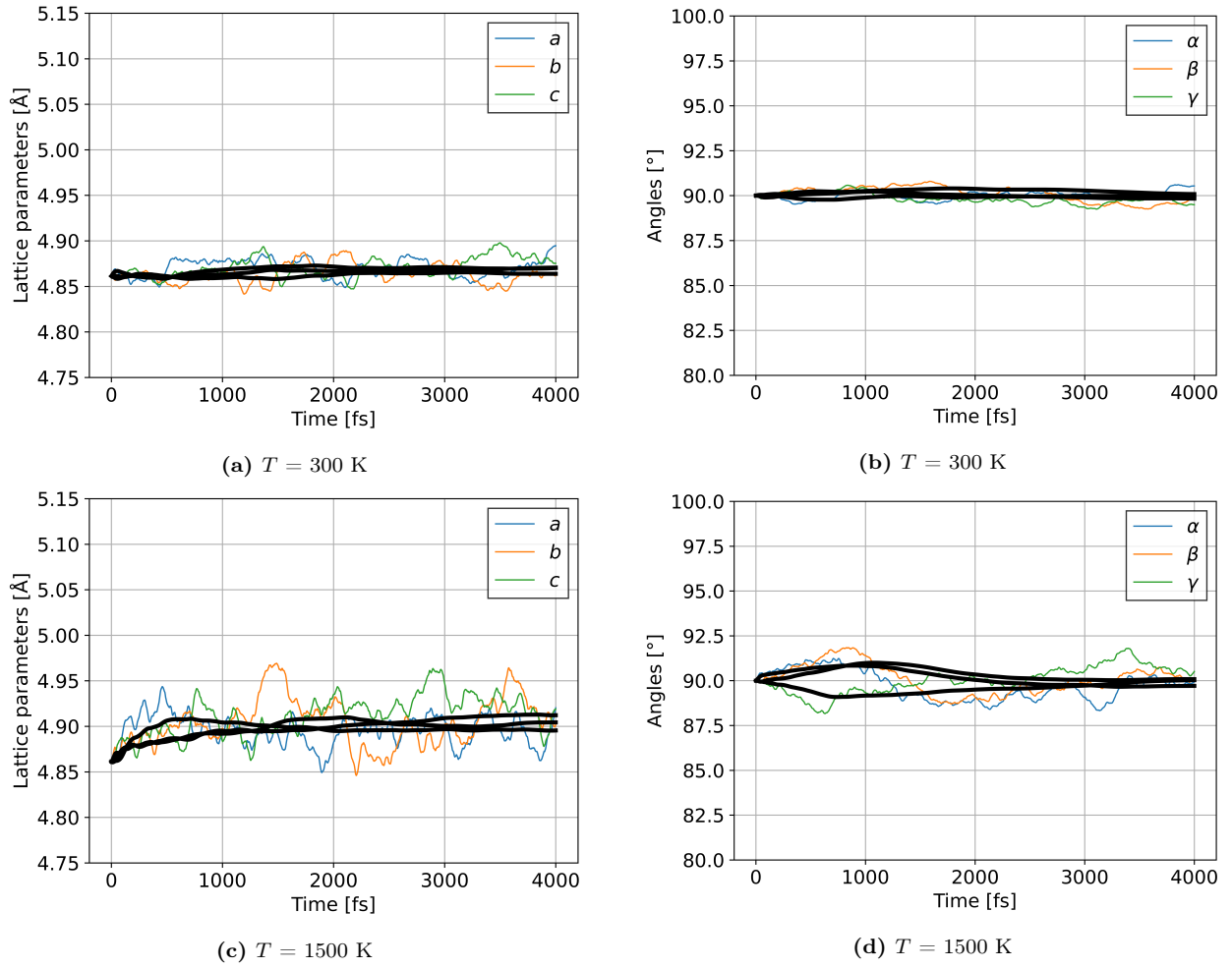


Figure 3: (Color online) (a) Lattice parameters of the UN unit cell at 300 K. (b) Angles between the lattice vectors of the UN unit cell at 300 K. (c) Lattice parameters of the UN unit cell at 1500 K. (d) Angles between the lattice vectors of the UN unit cell at 1500 K. Black thick lines correspond to running averages.

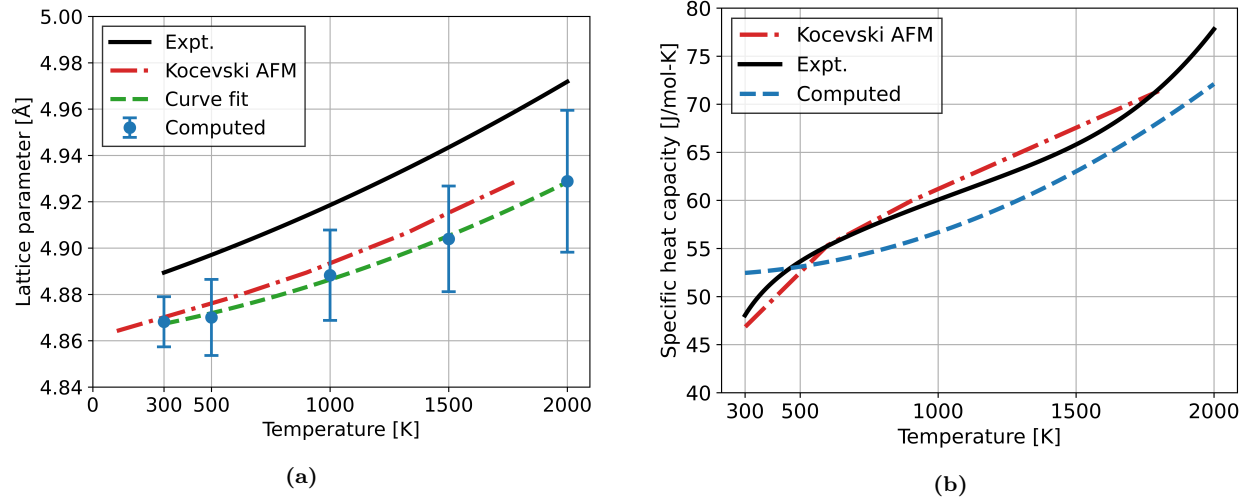


Figure 4: (Color online) (a) Calculated lattice constant of UN compared to the empirical correlation of Hayes *et al.* [26] and the AIMD data calculated by Kocevski *et al.* [16] for AFM UN. Error bars correspond to one standard deviation of the time average. (b) Fitted specific heat capacity of UN compared to the empirical correlation of Hayes *et al.* [27] and the AIMD data calculated by Kocevski *et al.* for AFM UN.

181 **4. Discussion**

182 Kocevski *et al.* [16] reported that AFM UN could be stabilized for a $2 \times 2 \times 2$ super-
183 cell. In contrast, our findings indicate that stabilizing AFM UN is not feasible for the larger
184 $3 \times 3 \times 3$ supercell, as the system transitions rapidly to a ferromagnetic state. Despite its
185 occasional use in prior studies, the AFM model of UN is fundamentally flawed in represent-
186 ing its paramagnetic state at high temperatures. In comparison, the AIMD+DLM approach
187 provides an accurate framework for simulating the paramagnetic state with minimal com-
188 putational overhead relative to conventional AIMD. Furthermore, the $3 \times 3 \times 3$ supercell is
189 more suitable for studying defects and diffusion mechanisms at finite temperatures, offering
190 a more representative model of the material’s behavior. We strongly recommend using the
191 AIMD+DLM methodology with the $3 \times 3 \times 3$ supercell to investigate the defect properties
192 of UN at finite temperatures.

193 The thermophysical predictions of this study, including the lattice parameter and specific
194 heat capacity (C_P), are in good agreement with those obtained from FM/AFM models of
195 UN. This observation suggests that the magnetic state may have a relatively minor influence
196 on the thermophysical properties of UN. However, this inference cannot be generalized to
197 other properties, such as the Debye temperature, which has been shown to be significantly
198 affected by the magnetic state of UN [28, 24]. Given these nuances, it is recommended to
199 employ the AIMD+DLM methodology to revisit other UN properties, particularly those that
200 are more sensitive to magnetic fluctuations.

201 The AIMD+DLM framework offers opportunities to study additional properties of UN
202 and other nuclear fuels, such as diffusion mechanisms and defect behavior, particularly those
203 linked to coupled magnetic and lattice dynamics. Its robust modeling of the paramagnetic
204 state can enhance understanding of nuclear fuel behavior at high temperatures, aiding the
205 development of more efficient and reliable nuclear materials.

206 **5. Conclusions**

207 This study demonstrates the application of *ab initio* molecular dynamics combined with
208 the disordered local moment model to simulate the paramagnetic state of UN. The key
209 conclusions drawn from this work are as follows:

- 210 • The AIMD+DLM approach effectively captures the paramagnetic state of UN, accu-
211 rately modeling the quasi-static magnetic fluctuations and their interaction with the
212 lattice dynamics. This method addresses the challenges posed by traditional DFT-
213 based approaches in simulating the high-temperature paramagnetic phase.
- 214 • The AIMD+DLM model predicts a cubic crystal structure for UN across the consid-
215 ered temperature range, consistent with experimental observations of its paramagnetic
216 phase.
- 217 • The calculated lattice parameter of UN is somewhat underestimated compared to the
218 empirical correlation of Hayes *et al.* across the entire temperature range. This under-
219 estimation is consistent with prior computational studies that treated UN in FM or
220 AFM states.

- 221 • The calculated specific heat capacity of UN is overestimated at low temperatures
222 (300–500 K) but slightly underestimated at higher temperatures $T > 500$ K, while
223 closely following the experimental trend.

224 **6. Acknowledgements**

225 This work is funded by the Westinghouse Electric Company. This research made use
226 of the resources of the High-Performance Computing Center at Idaho National Laboratory,
227 which is supported by the Office of Nuclear Energy of the U.S. Department of Energy and
228 the Nuclear Science User Facilities under Contract No. DE-AC07-05ID14517.

229 **7. Data Availability**

230 Data will be made available upon request to the corresponding author.

231 **References**

- 232 [1] J. Wallenius, Nitride fuels, Comprehensive Nuclear Materials 5 (2020) 88–101. [doi:10.1016/B978-0-12-803581-8.11694-7](https://doi.org/10.1016/B978-0-12-803581-8.11694-7).
- 233 [2] M. Uno, T. Nishi, M. Takano, Thermodynamic and thermophysical properties of
234 the actinide nitrides, Comprehensive Nuclear Materials: Second Edition (2020) 202–
235 231[doi:10.1016/B978-0-12-803581-8.11749-7](https://doi.org/10.1016/B978-0-12-803581-8.11749-7).
- 236 [3] N. A. Curry, An investigation of the magnetic structure of uranium nitride by neu-
237 tron diffraction, in: Proceedings of the Physical Society, Vol. 86, 1965. [doi:10.1088/0370-1328/86/6/304](https://doi.org/10.1088/0370-1328/86/6/304).
- 238 [4] M. Samsel-CzeKała, E. Talik, P. De, R. Troć, H. Misiorak, C. Sułkowski, Electronic
239 structure and magnetic and transport properties of single-crystalline UN, Physical Re-
240 view B 76 (2007) 144426. [doi:10.1103/PhysRevB.76.144426](https://doi.org/10.1103/PhysRevB.76.144426).
- 241 [5] I. A. Abrikosov, A. V. Ponomareva, P. Steneteg, S. A. Barannikova, B. Alling, Recent
242 progress in simulations of the paramagnetic state of magnetic materials (2016). [doi:10.1016/j.cossms.2015.07.003](https://doi.org/10.1016/j.cossms.2015.07.003).
- 243 [6] P. Steneteg, B. Alling, I. A. Abrikosov, Equation of state of paramagnetic CrN from
244 ab initio molecular dynamics, Physical Review B - Condensed Matter and Materials
245 Physics 85 (2012). [doi:10.1103/PhysRevB.85.144404](https://doi.org/10.1103/PhysRevB.85.144404).
- 246 [7] B. L. Gyorffy, A. J. Pindor, J. Staunton, G. M. Stocks, H. Winter, A first-principles
247 theory of ferromagnetic phase transitions in metals, Journal of Physics F: Metal Physics
248 15 (1985). [doi:10.1088/0305-4608/15/6/018](https://doi.org/10.1088/0305-4608/15/6/018).
- 249 [8] F. Giustino, Materials Modelling using Density Functional Theory: Properties and
250 Predictions, 1st Edition, Oxford University Press, 2014.

- 254 [9] G. Kotliar, D. Vollhardt, Strongly correlated materials: Insights from dynamical mean-
255 field theory (2004). [doi:10.1063/1.1712502](https://doi.org/10.1063/1.1712502).
- 256 [10] H. Liu, A. Claisse, S. C. Middleburgh, P. Olsson, Choosing the correct strong correlation
257 correction for U₃Si₂: Influence of magnetism, Journal of Nuclear Materials 527 (2019).
258 [doi:10.1016/j.jnucmat.2019.151828](https://doi.org/10.1016/j.jnucmat.2019.151828).
- 259 [11] S. Shousha, B. Beeler, Magnetism and finite-temperature effects in UZr₂: A density
260 functional theory analysis, Journal of Nuclear Materials 595 (2024) 155037. [doi:https://doi.org/10.1016/j.jnucmat.2024.155037](https://doi.org/10.1016/j.jnucmat.2024.155037).
- 262 [12] E. Mozafari, N. Shulumba, P. Steneteg, B. Alling, I. A. Abrikosov, Finite-temperature
263 elastic constants of paramagnetic materials within the disordered local moment picture
264 from ab initio molecular dynamics calculations, Physical Review B 94 (2016). [doi:10.1103/PhysRevB.94.054111](https://doi.org/10.1103/PhysRevB.94.054111).
- 266 [13] B. Alling, F. Körmann, B. Grabowski, A. Glensk, I. A. Abrikosov, J. Neugebauer, Strong
267 impact of lattice vibrations on electronic and magnetic properties of paramagnetic Fe
268 revealed by disordered local moments molecular dynamics, Physical Review B 93 (2016).
269 [doi:10.1103/PhysRevB.93.224411](https://doi.org/10.1103/PhysRevB.93.224411).
- 270 [14] V. Kocevski, D. A. Rehn, M. W. D. Cooper, D. A. Andersson, First-principles investi-
271 gation of uranium mononitride (UN): Effect of magnetic ordering, spin-orbit inter-
272 actions and exchange correlation functional, Journal of Nuclear Materials 559 (2022).
273 [doi:10.1016/j.jnucmat.2021.153401](https://doi.org/10.1016/j.jnucmat.2021.153401).
- 274 [15] A. Claisse, M. Klipfel, N. Lindbom, M. Freyss, P. Olsson, GGA+U study of uranium
275 mononitride: A comparison of the U-ramping and occupation matrix schemes and incor-
276 poration energies of fission products, Journal of Nuclear Materials 478 (2016) 119–124.
277 [doi:10.1016/j.jnucmat.2016.06.007](https://doi.org/10.1016/j.jnucmat.2016.06.007).
- 278 [16] V. Kocevski, D. A. Rehn, A. J. Terricabras, A. van Veelen, M. W. Cooper, S. W.
279 Paisner, S. C. Vogel, J. T. White, D. A. Andersson, Finite temperature properties of
280 uranium mononitride, Journal of Nuclear Materials 576 (2023) 154241. [doi:10.1016/j.jnucmat.2023.154241](https://doi.org/10.1016/j.jnucmat.2023.154241).
- 282 [17] G. Kresse, J. Hafner, Ab initio molecular dynamics for liquid metals, Physical Review
283 B 47 (1993). [doi:10.1103/PhysRevB.47.558](https://doi.org/10.1103/PhysRevB.47.558).
- 284 [18] G. Kresse, J. Furthmüller, Efficiency of ab-initio total energy calculations for metals
285 and semiconductors using a plane-wave basis set, Computational Materials Science 6
286 (1996). [doi:10.1016/0927-0256\(96\)00008-0](https://doi.org/10.1016/0927-0256(96)00008-0).
- 287 [19] G. Kresse, J. Furthmüller, Efficient iterative schemes for ab initio total-energy calcula-
288 tions using a plane-wave basis set, Physical Review B - Condensed Matter and Materials
289 Physics 54 (1996). [doi:10.1103/PhysRevB.54.11169](https://doi.org/10.1103/PhysRevB.54.11169).
- 290 [20] J. P. Perdew, K. Burke, M. Ernzerhof, Generalized gradient approximation made simple,
291 Physical Review Letters 77 (1996). [doi:10.1103/PhysRevLett.77.3865](https://doi.org/10.1103/PhysRevLett.77.3865).

- 292 [21] M. Methfessel, A. T. Paxton, High-precision sampling for Brillouin-zone integration in
293 metals, *Physical Review B* 40 (1989). [doi:10.1103/PhysRevB.40.3616](https://doi.org/10.1103/PhysRevB.40.3616).
- 294 [22] L. Yang, N. Kaltsoyannis, Incorporation of Kr and Xe in uranium mononitride: A
295 density functional theory study, *Journal of Physical Chemistry C* 125 (2021) 26999–
296 27008. [doi:10.1021/acs.jpcc.1c08523](https://doi.org/10.1021/acs.jpcc.1c08523).
- 297 [23] E. S. R. Gopal, *Specific Heats at Low Temperatures*, Springer US, 1966. [doi:10.1007/978-1-4684-9081-7_4](https://doi.org/10.1007/978-1-4684-9081-7_4).
- 299 [24] M. AbdulHameed, B. Beeler, C. O. Galvin, M. W. Cooper, Assessment of uranium
300 nitride interatomic potentials, *Journal of Nuclear Materials* (2024) 155247 [doi:https://doi.org/10.1016/j.jnucmat.2024.155247](https://doi.org/10.1016/j.jnucmat.2024.155247).
- 302 [25] A. Claisse, T. Schuler, D. A. Lopes, P. Olsson, Transport properties in dilute UN(X)
303 solid solutions (X = Xe, Kr), *Physical Review B* 94 (2016). [doi:10.1103/PhysRevB.94.174302](https://doi.org/10.1103/PhysRevB.94.174302).
- 305 [26] S. L. Hayes, J. K. Thomas, K. L. Peddicord, Material property correlations for uranium
306 mononitride I. physical properties, *Journal of Nuclear Materials* 171 (1990) 262–270.
- 307 [27] S. L. Hayes, J. K. Thomas, K. L. Peddicord, Material property correlations for uranium
308 mononitride IV. thermodynamic properties, *Journal of Nuclear Materials* 171 (1990)
309 300–318.
- 310 [28] H. L. Whaley, W. Fulkerson, R. A. Potter, Elastic moduli and Debye temperature of
311 polycrystalline uranium nitride by ultrasonic velocity measurements, *Journal of Nuclear
312 Materials* 31 (1969). [doi:10.1016/0022-3115\(69\)90234-7](https://doi.org/10.1016/0022-3115(69)90234-7).